

Beyond Open Vocabulary: Multimodal Prompting for Object Detection in Remote Sensing Images

Shuai Yang¹ Ziyue Huang¹ Jiaxin Chen¹ Qingjie Liu¹ Yunhong Wang¹

Abstract

Open-vocabulary object detection in remote sensing commonly relies on text-only prompting to specify target categories, implicitly assuming that inference-time category queries can be reliably grounded through pretraining-induced text–visual alignment. In practice, this assumption often breaks down in remote sensing scenarios due to task- and application-specific category semantics, resulting in unstable category specification under open-vocabulary settings. To address this limitation, we propose **RS-MPOD**, a multimodal open-vocabulary detection framework that reformulates category specification beyond text-only prompting by incorporating instance-grounded visual prompts, textual prompts, and their multimodal integration. RS-MPOD introduces a visual prompt encoder to extract appearance-based category cues from exemplar instances, enabling text-free category specification, and a multimodal fusion module to integrate visual and textual information when both modalities are available. Extensive experiments on standard, cross-dataset, and fine-grained remote sensing benchmarks show that visual prompting yields more reliable category specification under semantic ambiguity and distribution shifts, while multimodal prompting provides a flexible alternative that remains competitive when textual semantics are well aligned.

1. Introduction

Object detection is a fundamental task in remote sensing image analysis, where models are required to localize objects and assign category labels under large variations in spatial resolution, sensing conditions, and background complexity (Cheng & Han, 2016; Li et al., 2020b). With the

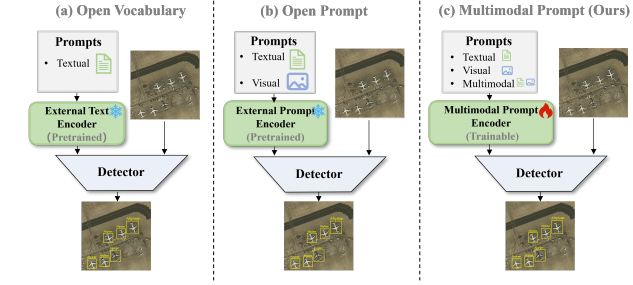


Figure 1. Prompting paradigms for object detection. (a) Open-vocabulary prompting only supports textual prompts. (b) Open prompt extends prompts to textual and visual inputs via an external pre-trained prompt encoder. (c) Our multimodal prompting jointly supports textual, visual, and multimodal prompts with trainable prompt encoders.

rapid development of remote sensing imaging technologies (Xia et al., 2018; Li et al., 2020a) and deep learning architectures (He et al., 2016; Ren et al., 2016; Vaswani et al., 2017), modern detectors have achieved strong performance across a wide range of challenging remote sensing scenarios (Xie et al., 2021; Yang et al., 2021; Lyu et al., 2022; Zeng et al., 2024). Despite these advances, most existing detectors remain constrained to fixed and closed category sets, which fundamentally limits their ability to recognize objects beyond the predefined training taxonomy.

To relax this limitation, the computer vision community has developed open-vocabulary object detection (OVOD) (Zareian et al., 2021), which formulates category prediction as a similarity-based matching problem between region-level visual representations and category embeddings. In practice, most OVOD methods derive category embeddings from category names or textual descriptions, and rely on large-scale image–text pretraining (Li et al., 2022b; Liu et al., 2024b; Cheng et al., 2024) or supervision from vision–language models (Gu et al., 2022; Zhao et al., 2022) to establish cross-modal correspondence, enabling category specification at inference time through textual prompts.

Recent studies have begun to extend open-vocabulary object detection to the remote sensing domain (Li et al., 2024; Wei et al., 2024), aiming to relax the closed-set constraint imposed by fixed category taxonomies. However, most ex-

¹School of Computer Science and Engineering, Beihang University, Beijing, China. Correspondence to: Qingjie Liu <qingjie.liu@buaa.edu.cn>.

isting approaches continue to rely almost exclusively on text-based category specification, implicitly assuming that inference-time category names can be reliably grounded to stable and discriminative visual concepts within the text–visual embedding space learned during vision–language pretraining (Fig. 1(a)). In remote sensing scenarios, this assumption is often violated. Unlike natural image benchmarks, category vocabularies and naming conventions in remote sensing are highly task- and application-dependent, and frequently diverge from those reflected in large-scale pretraining corpora. As a result, inference-time textual prompts may correspond to imprecise or biased visual concepts, making pretraining-induced text–visual alignment insufficient for reliable category specification.

This issue is further amplified under open-vocabulary settings, where category specification relies almost entirely on textual prompts without task-specific supervision, often leading to unstable or inconsistent detection behavior across datasets and category granularities. To alleviate the limitations of text-only prompting, recent work has explored incorporating visual exemplars as an alternative form of category specification (Huang et al., 2025), by encoding exemplar images as visual prompts using external pretrained models (Fig. 1(b)). However, such approaches typically treat textual and visual prompts as independent, unimodal inputs, and require additional alignment steps to project externally encoded visual prompts into the detector feature space. Moreover, they do not explicitly account for the potentially complementary information across different prompt modalities.

To address these limitations, we propose RS-MPOD, a multimodal prompting framework for open-vocabulary object detection that rethinks category specification beyond text-only prompting. RS-MPOD enables category specification through textual prompts, instance-grounded visual prompts, or their multimodal combination within a unified prompt-based detection framework (Fig. 1(c)). RS-MPOD is built upon GroundingDINO (Liu et al., 2024b), which provides a generic prompt-based detection architecture. Our design centers on category specification in prompt-based open-vocabulary detection, where visual features are encoded independently of category information and all category cues are introduced solely through prompt embeddings during decoding. To this end, we introduce a visual prompt encoder based on deformable attention (Zhu et al., 2021b) to extract instance-grounded appearance representations from annotated exemplar objects. These instance-level visual prompts provide a text-free mechanism for specifying categories based on visual similarity. At inference time, multiple visual prompts can be flexibly aggregated to form category-level representations, enabling open-vocabulary detection conditioned directly on visual exemplars. When both textual and visual cues are available, we further introduce a multi-

modal prompt fusion module that integrates prompts from different modalities into unified category representations, allowing the detector to exploit complementary semantic and appearance information.

Our contributions can be summarized as follows. (1) We identify the limitations of text-only category specification in remote sensing open-vocabulary object detection, and extend category specification to support visual exemplars and multimodal cues beyond category names. (2) We introduce a visual prompt encoder that extracts instance-grounded visual prompts from annotated exemplar objects to enable appearance-based category specification, together with a multimodal prompt fusion module that combines textual semantics with visual appearance cues to form unified category representations. (3) Extensive experiments on standard, cross-dataset, and fine-grained remote sensing benchmarks show that visual and multimodal category specification improves robustness under semantic ambiguity and distribution shifts, while remaining competitive when textual semantics are well aligned.

2. Related Work

2.1. OVOD in Natural Images

Open-vocabulary object detection (OVOD) casts category recognition as a similarity-based matching problem between region-level visual features and textual embeddings, enabling detectors to recognize categories beyond a fixed training taxonomy. Existing OVOD approaches in natural images can be broadly categorized into two paradigms according to how such cross-modal alignment is established.

The first paradigm explicitly incorporates cross-modal fusion mechanisms into the detector architecture and learns vision–language alignment through end-to-end training on large-scale image–text pairs (Li et al., 2022b; Yao et al., 2022; Minderer et al., 2022; Liu et al., 2024b; Cheng et al., 2024). These methods directly couple visual and textual streams during training, enabling strong cross-modal alignment, at the cost of increased reliance on large, well-curated image–text datasets and extensive training supervision.

The second paradigm builds upon pretrained vision–language models (VLMs) (Radford et al., 2021; Jia et al., 2021; Li et al., 2022a), which provide a shared semantic embedding space learned from large, web-scale image–text corpora. Within this paradigm, some approaches distill alignment knowledge from VLMs into detection models (Gu et al., 2022; Ma et al., 2022; Wang et al., 2023; Wu et al., 2023; Fu et al., 2025; Cao et al., 2025), while others exploit VLMs to generate pseudo-labels for unlabeled images (Zhao et al., 2022; Gao et al., 2022; Wang et al., 2024; Zhao et al., 2024), thereby transferring semantic structure into detection models through indirect supervision. While these

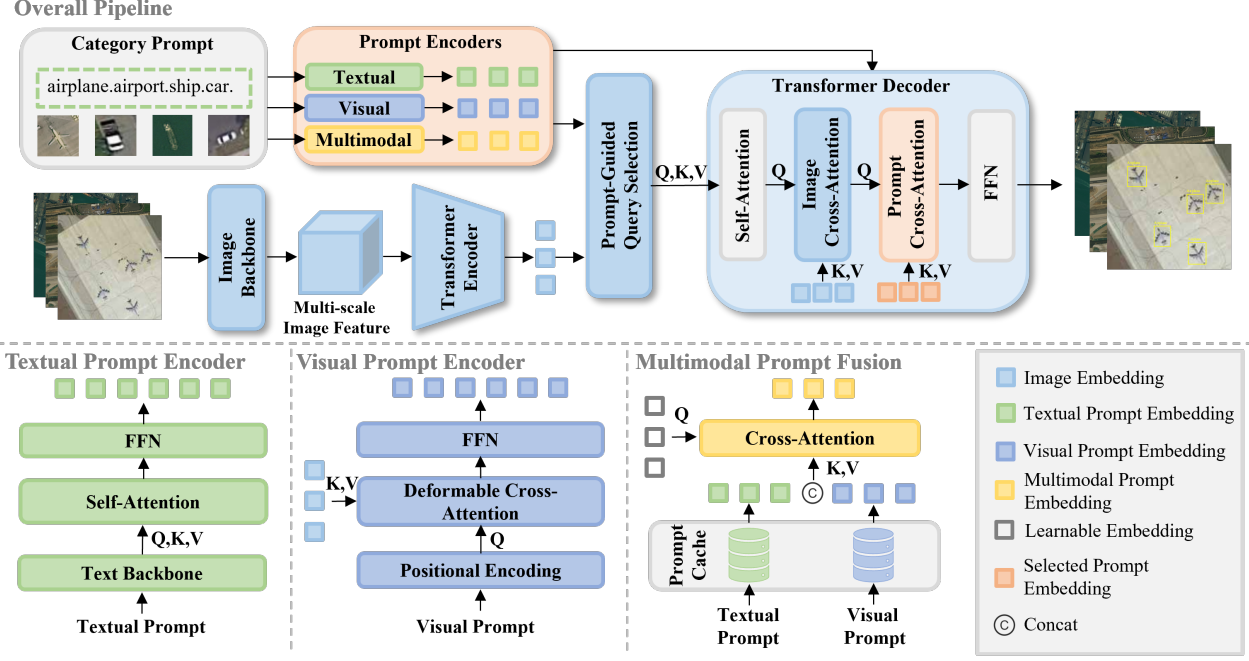


Figure 2. Overall framework of RS-MPOD. The detector is built upon GroundingDINO and supports textual prompting, visual prompting, and multimodal prompting within a unified detection pipeline. Prompt embeddings produced by different prompt encoders are used to condition query selection and cross-attention in the transformer decoder for category specification. The lower panels illustrate the designs of the textual prompt encoder, visual prompt encoder, and the multimodal prompt fusion module.

paradigms have proven effective for open-vocabulary detection in natural images, they typically rely on the implicit assumption that the vision–language alignment learned during pretraining or end-to-end training can be directly reused to support category specification at inference time.

2.2. OVOD in Remote Sensing Images

Several recent studies have explored extending open-vocabulary object detection to remote sensing imagery. OVA-DETR (Wei et al., 2024) enhances vision–language alignment by introducing cross-modal fusion between visual and textual features within the detector. CastDet (Li et al., 2024) leverages Remote-CLIP (Liu et al., 2024a) as a teacher model to generate pseudo-labels for unlabeled images, thereby expanding the effective label space for open-vocabulary detection in remote sensing. To further increase data diversity, LAE-DINO (Pan et al., 2025) constructs a large-scale remote sensing image–text corpus for pretraining, exposing detection models to a broader range of category descriptions. Despite these advances, most existing remote sensing OVOD methods primarily follow text-centric prompting and alignment strategies developed for natural images. Accordingly, category specification at inference time relies mainly on textual prompts together with vision–language alignment learned during pretraining. When applied to remote sensing datasets, variations in cat-

egory definitions and usage requirements across tasks can make such text-based category specification less reliable.

Beyond textual prompting, only a limited number of studies have explored the use of visual prompts in remote sensing. For instance, Huang et al. (Huang et al., 2025) employ visual prompts extracted offline using external pretrained models. However, visual prompts in these approaches are treated independently from textual prompts and require additional alignment to the detector feature space, without explicitly modeling interactions between different prompt modalities.

3. Method

3.1. Overview

The overall architecture of the proposed framework is illustrated in Fig. 2. Our detector is built upon GroundingDINO (Liu et al., 2024b), where visual features are extracted by an image backbone and transformer encoder, and category information is provided through prompt embeddings. Depending on the prompting configuration, prompt embeddings are generated by different prompt encoders and guide the detection process by conditioning query selection and cross-attention decoding, resulting in category and bounding box predictions.

The framework supports three prompting configurations within a unified detection pipeline. Textual prompting en-

codes category names into textual prompt embeddings. Visual prompting specifies categories using exemplar instances from annotated training data, which are processed by a visual prompt encoder to obtain instance-level appearance representations reused at inference time. Multimodal prompting further integrates textual and visual prompt embeddings through a multimodal prompt fusion module.

3.2. Prompt-Based Detection Framework

We build our detector upon GroundingDINO (Liu et al., 2024b) and consider open-vocabulary object detection under a prompt-conditioned detection framework. Given an input image I and category prompts $\mathcal{P} = \{P_k\}_{k=1}^K$, visual features are extracted by an image backbone as $F = \{F^{(l)}\}_{l=1}^L = B_v(I)$ and further processed by a transformer encoder to obtain encoded features $\tilde{F} = E_v(F)$. Conditioned on the category prompts, a set of queries $\{q_i\}$ is selected from the encoded visual features, which we denote abstractly as $\{q_i\} = \Phi(\tilde{F}, \mathcal{P})$, where $\Phi(\cdot)$ denotes a prompt-conditioned query initialization operation. These queries are then refined by a transformer decoder $D(\cdot)$, producing category-aware query representations $\hat{q}_i = D(q_i, \tilde{F})$ that are used for object classification and localization.

Each category k is specified by a prompt embedding P_k , and a decoded query \hat{q}_i is classified by comparing it against the category prompts. Bounding boxes are predicted from the decoded queries by an MLP head, i.e., $\hat{b}_i = h_{\text{box}}(\hat{q}_i)$.

Following a DETR-style formulation with bipartite matching, predictions are matched to ground-truth objects, and we denote by N the number of matched pairs. The classification loss is defined as:

$$\mathcal{L}_{\text{cls}} = -\frac{1}{N} \sum_{i=1}^N \log \frac{\exp(\cos(\hat{q}_i, P_{y_i})/\tau)}{\sum_{k=1}^K \exp(\cos(\hat{q}_i, P_k)/\tau)}, \quad (1)$$

where y_i is the ground-truth category label of the matched object and τ is a temperature parameter. Bounding boxes are supervised using \mathcal{L}_1 and GIoU losses:

$$\mathcal{L}_1 = \frac{1}{N} \sum_{i=1}^N \|\hat{b}_i - b_i\|_1, \quad (2)$$

$$\mathcal{L}_{\text{giou}} = \frac{1}{N} \sum_{i=1}^N (1 - \text{GIoU}(\hat{b}_i, b_i)), \quad (3)$$

where b_i denotes the ground-truth bounding box corresponding to the i -th matched prediction. The overall training objective is:

$$\mathcal{L} = \lambda_{\text{cls}} \mathcal{L}_{\text{cls}} + \lambda_1 \mathcal{L}_1 + \lambda_{\text{giou}} \mathcal{L}_{\text{giou}}. \quad (4)$$

where λ_{cls} , λ_1 , and λ_{giou} are scalar hyperparameters that balance the classification and box regression losses.

Within the prompt-based detection framework described above, we first describe the textual prompting setting, which follows the original GroundingDINO implementation.

Category specifications are provided as a set of textual prompts $T = \{t_k\}_{k=1}^K$, where each t_k denotes a category name. Each textual prompt is tokenized into n_k tokens and processed by a textual prompt encoder, consisting of a text backbone followed by self-attention and feed-forward layers. The encoder outputs token-level textual features $G_k = \{g_{k,j}\}_{j=1}^{n_k}$, which serve as the textual prompt embeddings for category k . For consistency with the prompt-conditioned detection framework, we denote the category prompt for textual prompting as $P_k = G_k$.

Compared to the original GroundingDINO, we remove the feature enhancement module in transformer encoder that injects textual information into visual encoding, so that visual features are encoded independently of prompt modalities and category information is introduced solely through the prompt set \mathcal{P} without modifying the detection pipeline.

3.3. Visual Prompt Encoder

Inspired by TRex2 (Jiang et al., 2024), we introduce a visual prompt encoder that constructs visual prompts from annotated object instances. These instance-grounded visual prompts serve as category prompts in the prompt-based detection framework, allowing object detection to be conditioned on visual appearance.

Given the encoded multi-scale visual features $\{\tilde{F}^{(l)}\}_{l=1}^L$ produced by the image backbone and transformer encoder, we construct visual prompts corresponding to categories present in the image. For an image containing a set of categories $\mathcal{C}_I \subseteq \{1, \dots, K\}$, we randomly sample one ground-truth bounding box b_k for each $k \in \mathcal{C}_I$. Each bounding box serves as a spatial prior for extracting visual information associated with category k .

The bounding box b_k is encoded by a positional encoding function and projected into the prompt space via an MLP:

$$e_k = \text{MLP}(\text{PE}(b_k)). \quad (5)$$

We introduce a learnable content vector c_k and concatenate it with the positional embedding to form a prompt query:

$$r_k = [e_k; c_k]. \quad (6)$$

Each prompt query r_k aggregates visual information from the multi-scale features through deformable attention:

$$z_k = \text{DeformAttn}(r_k, \{\tilde{F}^{(l)}\}_{l=1}^L), \quad (7)$$

and is processed by a feed-forward network to obtain the visual prompt embedding:

$$v_k = \text{FFN}(z_k). \quad (8)$$

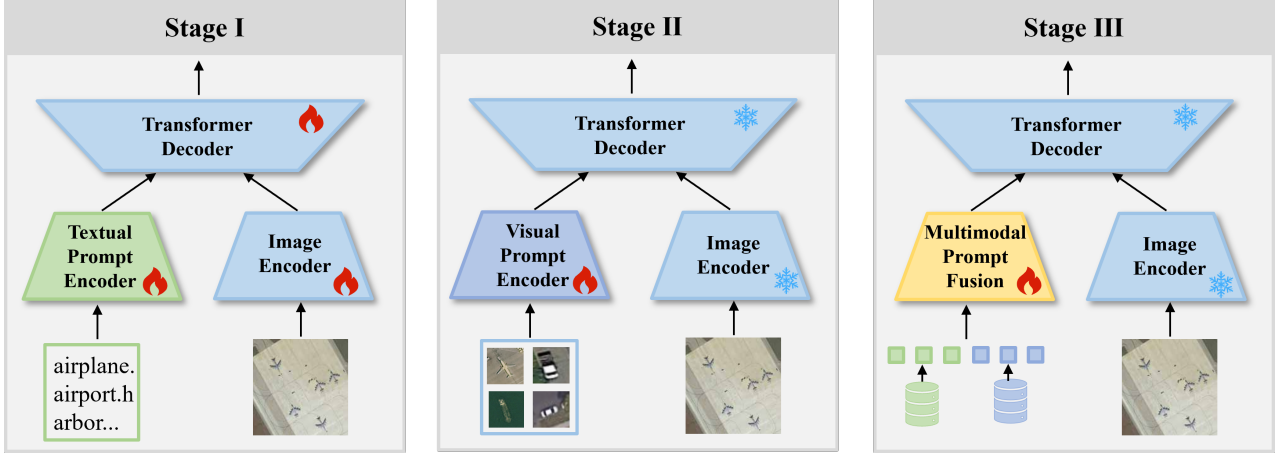


Figure 3. Stage-wise training strategy of RS-MPOD. The detector is first trained with textual prompts, followed by visual prompt encoder training and multimodal prompt fusion, with earlier components frozen in later stages. The image encoder consists of an image backbone and a transformer encoder.

The resulting embedding v_k serves as the visual prompt for category k , and we denote the corresponding category prompt as $P_k = v_k$. After training, the visual prompt encoder is applied to the training set to extract instance-level visual prompts for all annotated objects. For each category, the extracted visual prompts are collected into a category-specific cache. At inference time, a visual category prompt is obtained by sampling an arbitrary number of instance-level prompts from the corresponding cache and aggregating them by averaging, and the resulting representation is used as the visual category prompt P_k in the detection framework.

3.4. Multimodal Prompt Fusion Module

We introduce a multimodal prompt fusion module to combine textual and visual prompts within the prompt-based detection framework. In textual prompting, category prompts are represented as token-level feature sequences, whereas in visual prompting each category is represented by a single embedding. To integrate these heterogeneous representations, we adopt a lightweight fusion mechanism based on a single-layer multi-head cross-attention module.

For each category k , the textual prompt encoder produces token-level textual features $G_k = \{g_{k,j}\}_{j=1}^{n_k}$, while the visual prompt encoder produces a visual prompt embedding v_k . We introduce a learnable query vector u_k to aggregate information from both modalities. The textual tokens and the visual prompt are concatenated along the token dimension to form the key/value sequence:

$$S_k = [g_{k,1}, \dots, g_{k,n_k}; v_k]. \quad (9)$$

Cross-attention is applied with u_k as the query and S_k as both key and value:

$$\hat{u}_k = \text{CrossAttn}(u_k, S_k, S_k). \quad (10)$$

The fused embedding \hat{u}_k serves as the category prompt in the multimodal prompting setting, and we denote $P_k = \hat{u}_k$.

3.5. Stage-wise Training Strategy

We adopt a three-stage training strategy (Fig. 3) to decouple detector learning from prompt optimization: the detector learns general-purpose visual representations, while prompt-related modules encode category-specific cues from different modalities. This design avoids interference between prompt learning and stable detection feature formation.

Stage I: Detector training with textual prompts. We first train the detector with textual prompts to establish a stable detection backbone. All detector components and the textual prompt encoder are optimized in this stage. The resulting model provides shared visual representations for subsequent prompt learning.

Stage II: Visual prompt encoder. In the second stage, the detector trained in Stage I is frozen, and only the visual prompt encoder is optimized. After training, the visual prompt encoder is applied to the training set to construct category-specific visual prompt caches, which are used for visual and multimodal prompting in later stages.

Stage III: Multimodal prompt fusion module. In the final stage, the detector and prompt encoders remain fixed. The fusion module is trained using textual and visual prompts retrieved from caches to learn a multimodal category prompt.

4. Experiments

4.1. Datasets

We adopt LAE-1M (Pan et al., 2025) as the primary dataset for training. LAE-1M contains over 1,600 object categories

Table 1. Comparison with existing open-vocabulary detection methods. Results for GLIP, GroundingDINO, and LAE-DINO are taken from the LAE-DINO paper, while OpenRSD results are from its original paper. DIOR is evaluated using AP_{50} , and DOTA-v2.0 and LAE-80C are evaluated using mAP (AP_{50} is additionally reported for DOTA-v2.0). Unless otherwise specified, visual prompting uses 32 visual prompts, and multimodal prompting combines textual prompts with 32 visual prompts.

Method	Pretrain Dataset	Prompt	DIOR (AP_{50})	DOTA-v2.0 (mAP / AP_{50})	LAE-80C (mAP)
GLIP (Li et al., 2022b)	LAE-1M	text	82.8	43.0 / –	16.5
GroundingDINO (Liu et al., 2024b)	LAE-1M	text	83.6	46.0 / –	17.7
LAE-DINO (Pan et al., 2025)	LAE-1M	text	85.5	46.8 / –	20.2
OpenRSD (Huang et al., 2025)	ORSD+	text	76.7	– / 71.8	–
OpenRSD (Huang et al., 2025)	ORSD+	visual	76.7	– / 69.8	–
RS-MPOD (Ours)	LAE-1M	text	81.3	46.1 / 73.8	23.1
RS-MPOD (Ours)	LAE-1M	visual-32	76.2	44.1 / 70.1	20.1
RS-MPOD (Ours)	LAE-1M	multimodal	83.6	48.0 / 74.6	24.1

Table 2. Zero-shot cross-dataset generalization results on remote sensing benchmarks. Models are evaluated using AP_{50} under different prompting configurations.

Method	Prompt	HRRSD	VisDrone	AI-TOD	LEVIR
GroundingDINO (Liu et al., 2024b)	text	43.7	4.7	30.1	49.6
LAE-DINO (Pan et al., 2025)	text	42.8	2.3	31.5	50.8
RS-MPOD (Ours)	text	41.9	3.8	27.6	48.2
RS-MPOD (Ours)	visual-32	43.2	5.5	33.7	46.9
RS-MPOD (Ours)	multimodal	44.1	4.6	32.8	51.0

and is a large-scale remote sensing dataset designed for open-vocabulary object detection. It consists of two components: (i) **LAE-FOD**, which is curated from existing remote sensing detection datasets and annotated with high-quality human labels; and (ii) **LAE-COD**, which is automatically constructed from unlabeled image–text pairs through an automated pipeline, expanding the category set beyond manually annotated data.

4.2. Evaluation Benchmarks

We evaluate our method on multiple remote sensing detection benchmarks covering in-domain evaluation, cross-dataset generalization, and fine-grained category recognition. Specifically, DIOR (Li et al., 2020a) and DOTA-v2.0 (Xia et al., 2018) are used as representative benchmarks for in-domain open-vocabulary detection, while LAE-80C (Pan et al., 2025) is adopted to assess performance under a substantially larger category space. Cross-dataset generalization is evaluated on HRRSD (Zhang et al., 2019), VisDrone (Zhu et al., 2021a), AI-TOD (Wang et al., 2021), and LEVIR (Zou & Shi, 2017), which cover diverse sensing conditions and scene distributions. In addition, we evaluate open-vocabulary object detection on fine-grained remote sensing benchmarks, including SIMD (Haroon et al., 2020), MVRSD (Bai et al., 2024), MAR20 (Wenqi et al., 2024), and FGSD2021 (Zhang et al., 2021), where categories ex-

hibit subtle visual differences and more specialized category definitions. All evaluations are conducted using horizontal bounding boxes. AP_{50} is reported on DIOR and all cross-dataset and fine-grained benchmarks, while mAP is used on LAE-80C; for DOTA-v2.0, both mAP and AP_{50} are reported for fair comparison with prior work.

4.3. Implementation Details

We follow the three-stage training pipeline described in Sec. 3.5. Stages I and II are trained on the full LAE-1M dataset, including both LAE-FOD and LAE-COD. In Stage I, the text-prompt-based detector is trained for 24 epochs. In Stage II, the detector is frozen and only the visual prompt encoder is trained for 12 epochs. Stage III trains only the multimodal prompt fusion module for 12 epochs and uses the LAE-FOD subset, as visual prompts constructed from sparse or noisy categories in LAE-COD are less suitable for fusion training. All experiments are conducted using four NVIDIA RTX 3090 GPUs with distributed training.

4.4. Main Results

Comparison with existing methods. Table 1 compares our approach with representative open-vocabulary detectors. We include general-domain methods such as GLIP (Li

Table 3. Zero-shot cross-dataset generalization results on fine-grained remote sensing benchmarks. All models are evaluated using AP₅₀ under different prompting configurations.

Method	Prompt	SIMD	MVRSD	MAR20	FGSD2021
GroundingDINO (Liu et al., 2024b)	text	17.7	10.4	5.7	7.7
LAE-DINO (Pan et al., 2025)	text	20.5	4.6	3.7	4.7
RS-MPOD (Ours)	text	16.4	1.0	4.6	8.0
RS-MPOD (Ours)	visual-32	30.6	22.0	11.2	14.7
RS-MPOD (Ours)	multimodal	29.2	19.5	6.7	7.0

Table 4. Ablation study on different prompting configurations. DIOR is evaluated using AP₅₀, while DOTA-v2.0 and LAE-80C are evaluated using mAP. “visual-N” denotes the use of N visual prompts aggregated into a single category representation at inference time.

Prompt	DIOR (AP ₅₀)	DOTA-v2.0 (mAP)	LAE-80C (mAP)
text	81.3	46.1	23.1
visual-1	65.5	37.3	14.3
visual-4	73.6	43.4	17.9
visual-8	76.4	43.7	19.3
visual-16	75.7	44.2	19.6
visual-32	76.2	44.1	20.1
multimodal	83.6	48.0	24.1

et al., 2022b) and GroundingDINO (Liu et al., 2024b), as well as remote-sensing-specific approaches including LAE-DINO (Pan et al., 2025) and OpenRSD (Huang et al., 2025). This evaluation focuses on standard in-domain benchmarks, where category definitions and annotation protocols are consistent with the training data. Under text-only prompting, our model achieves 81.3% AP₅₀ on DIOR, 46.1% mAP on DOTA-v2.0, and 23.1% mAP on LAE-80C. Compared with LAE-DINO, this corresponds to slightly lower performance on DIOR and DOTA-v2.0, while yielding higher mAP on LAE-80C. With 32 visual prompts, our model reaches 76.2% AP₅₀ on DIOR and 70.1% AP₅₀ on DOTA-v2.0, achieving performance comparable to the visual-prompt results reported by OpenRSD. The multimodal configuration, which combines textual prompts with 32 visual prompts, provides the most stable overall performance across benchmarks. It obtains 48.0% mAP on DOTA-v2.0 and 24.1% mAP on LAE-80C, exceeding LAE-DINO by +1.2% and +3.9% mAP, respectively. On DIOR, multimodal prompting reaches 83.6% AP₅₀, matching the performance of GroundingDINO and remaining close to LAE-DINO. Overall, these results indicate that incorporating visual and multimodal prompting maintains competitive performance on standard benchmarks, while providing consistent gains when complementary category cues are available.

Cross-dataset generalization. Table 2 reports zero-shot

Table 5. Effect of freezing the detector during visual prompt encoder training. “Unfrozen” and “Frozen” indicate whether detector parameters are updated during training.

Condition	Prompt	DIOR (AP ₅₀)	DOTA-v2.0 (mAP)
Unfrozen	visual-32	60.9	34.9
Frozen	visual-32	76.2	44.1

Table 6. Comparison of fusion strategies for combining textual and visual prompts. The “Avg” baseline represents simple averaging of textual and visual prompts, whereas “Fusion” denotes our proposed module for learned multimodal integration.

Strategy	Prompt	DIOR (AP ₅₀)	DOTA-v2.0 (mAP)
Avg	multimodal	79.8	45.4
Fusion	multimodal	83.6	48.0

detection results on several external datasets. Several consistent patterns can be observed across cross-dataset settings. Within RS-MPOD, visual prompting achieves higher or more stable performance than textual prompting on most benchmarks, with particularly notable gains on AI-TOD (+6.1% AP₅₀). On these datasets, RS-MPOD with visual prompting also achieves performance comparable to or exceeding representative text-prompt-based methods such as GroundingDINO and LAE-DINO. This behavior differs from the in-domain results, where textual prompting generally performs better. A consistent observation is that the effectiveness of textual prompting varies substantially across datasets, suggesting that inference-time category specifications may not consistently align with the text–visual alignment learned during pretraining under distribution shifts. By contrast, visual prompts rely on appearance cues extracted from exemplar instances to specify categories based on visual similarity. Multimodal prompting provides additional gains on some datasets, such as HRRSD and LEVIR (e.g., +2.8% AP₅₀ on LEVIR). On VisDrone and AI-TOD, multimodal prompting performs comparably to or slightly below visual-only prompting, indicating that instance-level appearance cues play a dominant role in cross-dataset generalization in these cases, particularly when category semantics differ substantially across datasets.

Fine-grained cross-dataset generalization. Table 3 reports zero-shot detection results on several fine-grained remote sensing benchmarks. Compared with the general cross-dataset setting, fine-grained benchmarks exhibit a substantially larger performance gap between textual and visual prompting. Across all fine-grained datasets, visual prompting achieves consistently higher performance than text-only prompting, with particularly large gains of +14.2% AP₅₀ on SIMD, +21.0% AP₅₀ on MVRSD, +6.6% AP₅₀ on MAR20, and +6.7% AP₅₀ on FGSD2021. On these benchmarks, RS-MPOD with visual prompting also substantially outperforms representative text-prompt-based methods such as GroundingDINO and LAE-DINO. Multimodal prompting remains competitive across all benchmarks, while performing comparably to or slightly below visual-only prompting on most fine-grained datasets, as poorly aligned textual cues can introduce additional semantic noise during fusion. Overall, these results indicate that under fine-grained cross-dataset evaluation, discrepancies between pretraining semantics and inference-time category definitions become more pronounced, under which category specification based on instance-level appearance cues remains more stable than text-only prompting.

4.5. Ablation Experiments

Results under different prompting configurations. Table 4 reports the performance under different prompting configurations. Several consistent patterns can be observed across benchmarks. First, using a single visual prompt results in notably lower performance, indicating that a single exemplar provides limited coverage of intra-class appearance variations. Second, performance improves steadily as the number of visual prompts increases: increasing the number of visual prompts from Visual-1 to Visual-32 leads to gains of +10.7% AP₅₀ on DIOR, +6.8% mAP on DOTA-v2.0, and +5.8% mAP on LAE-80C. This trend suggests that aggregating multiple exemplar instances enables the visual prompt encoder to form more representative category-level appearance cues. Third, even with multiple visual prompts, the visual-only configuration performs slightly below the text-only baseline. This difference reflects the distinct roles of textual and visual prompting in category specification. Textual prompts provide category identifiers that directly correspond to benchmark labels, whereas visual prompts rely on a limited set of exemplar appearances, which may be insufficient to fully characterize category boundaries. Finally, the multimodal configuration consistently achieves the strongest performance across benchmarks, outperforming the text-only baseline by +2.3% AP₅₀ on DIOR, +1.9% mAP on DOTA-v2.0, and +1.0% mAP on LAE-80C. These results confirm that textual and visual prompts provide complementary category cues, and their integration leads to more effective category specification.

Effect of freezing the detector during visual prompt encoder training. Table 5 examines the effect of freezing the detector when training the visual prompt encoder. In the first configuration, the detector and the visual prompt encoder are jointly optimized, with each iteration conditioned on either textual or visual prompts. In the second configuration, all detector parameters are frozen and only the visual prompt encoder is updated. Freezing the detector leads to substantially better performance, improving DIOR AP₅₀ by +15.3% and DOTA-v2.0 mAP by +9.2%. This result indicates that learning visual prompts benefits from a stable category-querying space. When the detector continues to update, both visual and query representations change simultaneously, making it difficult for the visual prompt encoder to adapt stably. By freezing the detector, the visual prompt encoder is trained with fixed visual representations and a stable querying mechanism, enabling more effective instance-grounded prompt embeddings.

Effect of fusion strategy for combining textual and visual prompts. Table 6 compares the proposed multimodal prompt fusion module with a non-learnable baseline. In the baseline, the visual prompt for each category is directly added to the token-level textual features, and the resulting features are averaged to obtain a category representation. Under the same textual+Visual-32 inference setting, the proposed fusion module consistently outperforms the non-learnable baseline, improving DIOR AP₅₀ by +3.8% and DOTA-v2.0 mAP by +2.6%. This result suggests that effectively combining textual and visual prompts requires a dedicated fusion mechanism that accounts for their different structures and roles in category specification, rather than treating them as interchangeable features through averaging.

5. Conclusion

In this work, we focus on category specification in open-vocabulary object detection for remote sensing, where inference-time category definitions and granularity often differ from training data, challenging the reliability of text-only prompting. Our experiments show that although text-only prompting can perform well when inference-time category semantics align with learned text-visual correspondence, its effectiveness degrades under cross-dataset shifts and becomes particularly fragile in fine-grained settings. To address this limitation, we propose RS-MPOD, a multimodal prompting framework that enables category specification through instance-grounded visual exemplars and their integration with textual prompts. Results across in-domain, cross-dataset, and fine-grained benchmarks demonstrate that visual prompting yields more stable category cues under semantic or distribution shifts, while multimodal prompting provides a flexible and robust alternative when both textual and visual cues are available.

Impact Statement

This paper presents work whose goal is to advance the field of Machine Learning. There are many potential societal consequences of our work, none which we feel must be specifically highlighted here.

References

Bai, D., Yu, Y., Song, L., Cheng, B., and Gao, H. Construction and validation of remote sensing image dataset for fine-grained detection of military vehicles. *J. Image Graph.*, 29(12):3564–3577, 2024.

Cao, G., Wang, T., Huang, W., Lan, X., Zhang, J., and Jiang, D. Open-det: An efficient learning framework for open-ended detection. In *International Conference on Machine Learning*, pp. 6654–6674, 2025.

Cheng, G. and Han, J. A survey on object detection in optical remote sensing images. *ISPRS Journal of Photogrammetry and Remote Sensing*, 117:11–28, 2016.

Cheng, T., Song, L., Ge, Y., Liu, W., Wang, X., and Shan, Y. Yolo-world: Real-time open-vocabulary object detection. In *Proceedings of the IEEE/CVF Conference on Computer Vision and Pattern Recognition*, pp. 16901–16911, 2024.

Fu, S., Yan, J., Yang, Q., Wei, X., Xie, X., and Zheng, W.-S. A hierarchical semantic distillation framework for open-vocabulary object detection. *arXiv preprint arXiv:2503.10152*, 2025.

Gao, M., Xing, C., Niebles, J. C., Li, J., Xu, R., Liu, W., and Xiong, C. Open vocabulary object detection with pseudo bounding-box labels. In *European Conference on Computer Vision*, pp. 266–282. Springer, 2022.

Gu, X., Lin, T.-Y., Kuo, W., and Cui, Y. Open-vocabulary object detection via vision and language knowledge distillation. In *International Conference on Learning Representations*, pp. 15099–15118, 2022.

Haroon, M., Shahzad, M., and Fraz, M. M. Multisized object detection using spaceborne optical imagery. *IEEE Journal of Selected Topics in Applied Earth Observations and Remote Sensing*, 13:3032–3046, 2020.

He, K., Zhang, X., Ren, S., and Sun, J. Deep residual learning for image recognition. In *Proceedings of the IEEE Conference on Computer Vision and Pattern Recognition*, pp. 770–778, 2016.

Huang, Z., Feng, Y., Liu, Z., Yang, S., Liu, Q., and Wang, Y. Openrsd: Towards open-prompts for object detection in remote sensing images. In *Proceedings of the IEEE/CVF International Conference on Computer Vision*, pp. 8384–8394, 2025.

Jia, C., Yang, Y., Xia, Y., Chen, Y.-T., Parekh, Z., Pham, H., Le, Q., Sung, Y.-H., Li, Z., and Duerig, T. Scaling up visual and vision-language representation learning with noisy text supervision. In *International Conference on Machine Learning*, pp. 4904–4916. PMLR, 2021.

Jiang, Q., Li, F., Zeng, Z., Ren, T., Liu, S., and Zhang, L. T-rex2: Towards generic object detection via text-visual prompt synergy. In *European Conference on Computer Vision*, pp. 38–57. Springer, 2024.

Li, J., Li, D., Xiong, C., and Hoi, S. Blip: Bootstrapping language-image pre-training for unified vision-language understanding and generation. In *International Conference on Machine Learning*, pp. 12888–12900. PMLR, 2022a.

Li, K., Wan, G., Cheng, G., Meng, L., and Han, J. Object detection in optical remote sensing images: A survey and a new benchmark. *ISPRS Journal of Photogrammetry and Remote Sensing*, 159:296–307, 2020a.

Li, K., Wan, G., Cheng, G., Meng, L., and Han, J. Object detection in optical remote sensing images: A survey and a new benchmark. *ISPRS Journal of Photogrammetry and Remote Sensing*, 159:296–307, 2020b.

Li, L. H., Zhang, P., Zhang, H., Yang, J., Li, C., Zhong, Y., Wang, L., Yuan, L., Zhang, L., Hwang, J.-N., et al. Grounded language-image pre-training. In *Proceedings of the IEEE/CVF Conference on Computer Vision and Pattern Recognition*, pp. 10965–10975, 2022b.

Li, Y., Guo, W., Yang, X., Liao, N., He, D., Zhou, J., and Yu, W. Toward open vocabulary aerial object detection with clip-activated student-teacher learning. In *European Conference on Computer Vision*, pp. 431–448. Springer, 2024.

Liu, F., Chen, D., Guan, Z., Zhou, X., Zhu, J., Ye, Q., Fu, L., and Zhou, J. Remoteclip: A vision language foundation model for remote sensing. *IEEE Transactions on Geoscience and Remote Sensing*, 62:1–16, 2024a.

Liu, S., Zeng, Z., Ren, T., Li, F., Zhang, H., Yang, J., Jiang, Q., Li, C., Yang, J., Su, H., et al. Grounding dino: Marrying dino with grounded pre-training for open-set object detection. In *European Conference on Computer Vision*, pp. 38–55. Springer, 2024b.

Lyu, C., Zhang, W., Huang, H., Zhou, Y., Wang, Y., Liu, Y., Zhang, S., and Chen, K. Rtdet: An empirical study of designing real-time object detectors. *ArXiv Preprint ArXiv:2212.07784*, 2022.

Ma, Z., Luo, G., Gao, J., Li, L., Chen, Y., Wang, S., Zhang, C., and Hu, W. Open-vocabulary one-stage detection with hierarchical visual-language knowledge distillation. In

Proceedings of the IEEE/CVF Conference on Computer Vision and Pattern Recognition, pp. 14074–14083, 2022.

Minderer, M., Gritsenko, A., Stone, A., Neumann, M., Weissenborn, D., Dosovitskiy, A., Mahendran, A., Arnab, A., Dehghani, M., Shen, Z., et al. Simple open-vocabulary object detection. In *European Conference on Computer Vision*, pp. 728–755. Springer, 2022.

Pan, J., Liu, Y., Fu, Y., Ma, M., Li, J., Paudel, D. P., Van Gool, L., and Huang, X. Locate anything on earth: Advancing open-vocabulary object detection for remote sensing community. In *Proceedings of the AAAI Conference on Artificial Intelligence*, volume 39, pp. 6281–6289, 2025.

Radford, A., Kim, J. W., Hallacy, C., Ramesh, A., Goh, G., Agarwal, S., Sastry, G., Askell, A., Mishkin, P., Clark, J., et al. Learning transferable visual models from natural language supervision. In *International Conference on Machine Learning*, pp. 8748–8763. PMLR, 2021.

Ren, S., He, K., Girshick, R., and Sun, J. Faster r-cnn: Towards real-time object detection with region proposal networks. *IEEE Transactions on Pattern Analysis and Machine Intelligence*, 39(6):1137–1149, 2016.

Vaswani, A., Shazeer, N., Parmar, N., Uszkoreit, J., Jones, L., Gomez, A. N., Kaiser, Ł., and Polosukhin, I. Attention is all you need. *Advances in Neural Information Processing Systems*, 30, 2017.

Wang, J., Yang, W., Guo, H., Zhang, R., and Xia, G.-S. Tiny object detection in aerial images. In *International Conference on Pattern Recognition*, pp. 3791–3798. IEEE, 2021.

Wang, K., Cheng, L., Chen, W., Zhang, P., Lin, L., Zhou, F., and Li, G. Marvelovd: Marrying object recognition and vision-language models for robust open-vocabulary object detection. In *European Conference on Computer Vision*, pp. 106–122. Springer, 2024.

Wang, L., Liu, Y., Du, P., Ding, Z., Liao, Y., Qi, Q., Chen, B., and Liu, S. Object-aware distillation pyramid for open-vocabulary object detection. In *Proceedings of the IEEE/CVF Conference on Computer Vision and Pattern Recognition*, pp. 11186–11196, 2023.

Wei, G., Yuan, X., Liu, Y., Shang, Z., Yao, K., Li, C., Yan, Q., Zhao, C., Zhang, H., and Xiao, R. Ova-detr: Open vocabulary aerial object detection using image-text alignment and fusion. *arXiv e-prints*, pp. arXiv–2408, 2024.

Wenqi, Y., Gong, C., Meijun, W., Yanqing, Y., Xingxing, X., Xiwen, Y., and Junwei, H. Mar20: A benchmark for military aircraft recognition in remote sensing images.

National Remote Sensing Bulletin, 27(12):2688–2696, 2024.

Wu, S., Zhang, W., Xu, L., Jin, S., Li, X., Liu, W., and Loy, C. C. Clipself: Vision transformer distills itself for open-vocabulary dense prediction. In *International Conference on Learning Representations*, pp. 35483–35502, 2023.

Xia, G.-S., Bai, X., Ding, J., Zhu, Z., Belongie, S., Luo, J., Datcu, M., Pelillo, M., and Zhang, L. Dota: A large-scale dataset for object detection in aerial images. In *Proceedings of the IEEE Conference on Computer Vision and Pattern Recognition*, pp. 3974–3983, 2018.

Xie, X., Cheng, G., Wang, J., Yao, X., and Han, J. Oriented r-cnn for object detection. In *Proceedings of the IEEE/CVF International Conference on Computer Vision*, pp. 3520–3529, 2021.

Yang, X., Yan, J., Feng, Z., and He, T. R3det: Refined single-stage detector with feature refinement for rotating object. In *Proceedings of the AAAI Conference on Artificial Intelligence*, volume 35, pp. 3163–3171, 2021.

Yao, L., Han, J., Wen, Y., Liang, X., Xu, D., Zhang, W., Li, Z., Xu, C., and Xu, H. Detclip: Dictionary-enriched visual-concept paralleled pre-training for open-world detection. *Advances in Neural Information Processing Systems*, 35:9125–9138, 2022.

Zareian, A., Rosa, K. D., Hu, D. H., and Chang, S.-F. Open-vocabulary object detection using captions. In *Proceedings of the IEEE/CVF Conference on Computer Vision and Pattern Recognition*, pp. 14393–14402, 2021.

Zeng, Y., Chen, Y., Yang, X., Li, Q., and Yan, J. Ars-detr: Aspect ratio-sensitive detection transformer for aerial oriented object detection. *IEEE Transactions on Geoscience and Remote Sensing*, 62:1–15, 2024.

Zhang, F., Wang, X., Zhou, S., Wang, Y., and Hou, Y. Arbitrary-oriented ship detection through center-head point extraction. *IEEE Transactions on Geoscience and Remote Sensing*, 60:1–14, 2021.

Zhang, Y., Yuan, Y., Feng, Y., and Lu, X. Hierarchical and robust convolutional neural network for very high-resolution remote sensing object detection. *IEEE Transactions on Geoscience and Remote Sensing*, 57(8):5535–5548, 2019.

Zhao, S., Zhang, Z., Schulter, S., Zhao, L., Vijay Kumar, B., Stathopoulos, A., Chandraker, M., and Metaxas, D. N. Exploiting unlabeled data with vision and language models for object detection. In *European Conference on Computer Vision*, pp. 159–175. Springer, 2022.

Zhao, S., Schulter, S., Zhao, L., Zhang, Z., Suh, Y., Chander, M., Metaxas, D. N., et al. Taming self-training for open-vocabulary object detection. In *Proceedings of the IEEE/CVF Conference on Computer Vision and Pattern Recognition*, pp. 13938–13947, 2024.

Zhu, P., Wen, L., Du, D., Bian, X., Fan, H., Hu, Q., and Ling, H. Detection and tracking meet drones challenge. *IEEE Transactions on Pattern Analysis and Machine Intelligence*, 44(11):7380–7399, 2021a.

Zhu, X., Su, W., Lu, L., Li, B., Wang, X., and Dai, J. Deformable detr: Deformable transformers for end-to-end object detection. In *International Conference on Learning Representations*, pp. 894–909, 2021b.

Zou, Z. and Shi, Z. Random access memories: A new paradigm for target detection in high resolution aerial remote sensing images. *IEEE Transactions on Image Processing*, 27(3):1100–1111, 2017.

A. Appendix for Experiments.

A.1. Fine-Grained Category Definitions and Mappings

This appendix summarizes the category definitions of the fine-grained remote sensing datasets used in our experiments, including SIMD (Haroon et al., 2020), MVRSD (Bai et al., 2024), MAR20 (Wenqi et al., 2024), and FGSD2021 (Zhang et al., 2021). These datasets adopt specialized or application-specific taxonomies that are not commonly used in standard object detection benchmarks. For clarity and reproducibility, we list the category names of all fine-grained datasets in Table 7. In addition, for datasets with non-semantic identifiers or overly specialized class names that are difficult to specify using textual prompts, we adopt category name normalization or functional grouping for analysis. These modifications are limited to category naming for semantic interpretability and textual prompting, while the original annotations, instance assignments, and evaluation protocols remain unchanged.

Table 7. Category definitions of fine-grained remote sensing datasets used in this work.

Dataset	Category Names
SIMD	Van, Long Vehicle, Bus, Airliner, Propeller Aircraft, Trainer Aircraft, Chartered Aircraft, Fighter Aircraft, Helicopter, Boat, Stair Truck, Pushback Truck, Car, Truck, Others
MVRSD	Small Military Vehicles, Large Military Vehicles, Armored Fighting Vehicles, Military Construction Vehicles, Civilian Vehicles
MAR20	Su-35 Fighter, Tu-160 Bomber, Tu-22 Bomber, Tu-95 Bomber, Su-34 Fighter-Bomber, Su-24 Fighter-Bomber, C-130 Transport Aircraft, C-17 Transport Aircraft, F-22 Fighter, F-16 Fighter, E-3 AWACS, B-52 Bomber, P-3C Anti-Submarine Aircraft, B-1B Bomber, E-8 JSTARS, F-15 Fighter, KC-135 Aerial Refueling Aircraft, C-5 Transport Aircraft, F/A-18 Fighter-Attack Aircraft, KC-10 Aerial Refueling Aircraft
FGSD2021	Aircraft Carrier, Cruiser, Destroyer, Frigate, Amphibious Ship, Support Ship, Submarine, Other

Table 8. Mapping from original class names to updated category names for fine-grained aircraft and ship datasets.

MAR20 (Aircraft)		FGSD2021 (Ships)	
Original Class Name	Updated Category Name	Original Class Name	Updated Category Name
A1	Su-35 Fighter	Ticonderoga-class	Cruiser
A2	Tu-160 Bomber	Perry-class	Frigate
A3	Tu-22 Bomber	Freedom-class	Frigate
A4	Tu-95 Bomber	Independence-class	Frigate
A5	Su-34 Fighter-Bomber	Arleigh Burke-class	Destroyer
A6	Su-24 Fighter-Bomber	Aircraft Carrier	Aircraft Carrier
A7	C-130 Transport Aircraft	Submarine	Submarine
A8	C-17 Transport Aircraft	Tarawa-class	Amphibious Ship
A9	C-5 Transport Aircraft	Austin-class	Amphibious Ship
A10	F-16 Fighter	Wasp-class	Amphibious Ship
A11	E-3 AWACS	Whidbey Island-class	Amphibious Ship
A12	B-52 Bomber	San Antonio-class	Amphibious Ship
A13	P-3C Anti-Submarine Aircraft	Newport-class	Amphibious Ship
A14	B-1B Bomber	Kaiser-class	Support Ship
A15	E-8 JSTARS	Avenger-class	Support Ship
A16	F-15 Fighter	Hope-class	Support Ship
A17	KC-135 Aerial Refueling Aircraft	Supply-class	Support Ship
A18	F-22 Fighter	Mercy-class	Support Ship
A19	F/A-18 Fighter-Attack Aircraft	Lewis and Clark-class	Support Ship
A20	KC-10 Aerial Refueling Aircraft	Other	Other

Both MAR20 and FGSD2021 contain highly fine-grained categories with specialized naming conventions. For MAR20, abstract identifiers are replaced with semantically meaningful aircraft type names, while FGSD2021 ship classes are grouped into broader functional categories for analysis, as summarized in Table 8. These adjustments affect only category name representation and do not alter the underlying annotation structure or evaluation procedures.

A.2. Appendix for Ablation Experiments.

Effect of the number of sampled instances for constructing visual prompts. Table 9 analyzes how the number of sampled instances per category during training influences the performance of the visual prompt encoder. Across different inference configurations, sampling a single instance per category in each training iteration consistently yields the strongest performance on both DIOR and DOTA-v2.0. Increasing the number of sampled instances to four or eight per category does not provide additional gains and in some cases leads to slightly lower AP₅₀/mAP. This behavior suggests that sampling a single instance introduces higher variability in prompt construction across training iterations, whereas sampling multiple instances simultaneously results in more stable but less diverse prompts. Such increased variability may serve as an implicit regularization mechanism, improving the robustness of the learned instance-grounded visual prompts.

Table 9. Effect of the number of sampled instances per category during training for visual prompt construction.

Prompt	DIOR (AP ₅₀)			DOTA-v2.0 (mAP)		
	1	4	8	1	4	8
visual-1	65.5	59.3	57.4	37.3	35.8	32.8
visual-4	73.6	70.6	72.7	43.4	40.2	42.4
visual-8	76.4	75.8	74.5	43.7	41.9	42.2
visual-16	75.7	75.3	75.6	44.2	43.5	43.9
visual-32	76.2	75.5	76.1	44.1	43.5	43.4

Effect of the number of visual prompts used for training the fusion module. Table 10 examines how the number of visual prompts provided during training affects the multimodal prompt fusion module. We consider three training strategies: using a single visual prompt, randomly sampling a variable number of prompts, and using the full set of 32 visual prompts. All models are evaluated under the same textual+Visual-32 inference configuration. Training with the full set of 32 visual prompts consistently yields the best performance across benchmarks. Reducing the number of visual prompts during training results in lower AP₅₀/mAP, indicating that exposing the fusion module to a broader and more diverse set of visual prompts is important for learning effective multimodal category representations.

Table 10. Effect of the number of visual prompts used to train the multimodal fusion module. During training, “visual-r” denotes random sampling of visual prompts.

Training prompt	Inference prompt	DIOR (AP ₅₀)	DOTA-v2.0 (mAP)
visual-1	visual-32	81.4	47.3
visual-r	visual-32	83.0	47.6
visual-32	visual-32	83.6	48.0

B. Appendix for Results Visualization.

Figure 4 provides a qualitative comparison of detection results under different prompting strategies, illustrating how textual, visual, and multimodal prompts behave under varying semantic conditions. In the first row, ship detection results are shown for a scenario where the evaluation dataset uses the category name *boat*, while large-scale pretraining corpora predominantly employ the term *ship*. Under text-only prompting, this semantic mismatch leads the detector to confuse boats with visually related categories such as *airliner*, whereas visual prompting correctly localizes and classifies the targets by relying on instance-level appearance cues. In the second row, the model is evaluated on car detection in a setting where the concept of *car* is weakly represented in pretraining data, but visually similar categories such as *van* are more prevalent. As a result, text-only prompting tends to misclassify cars as vans, while visual prompting reduces this confusion by grounding category specification in visual exemplars. In contrast, the third row shows helicopter detection in a scenario where textual

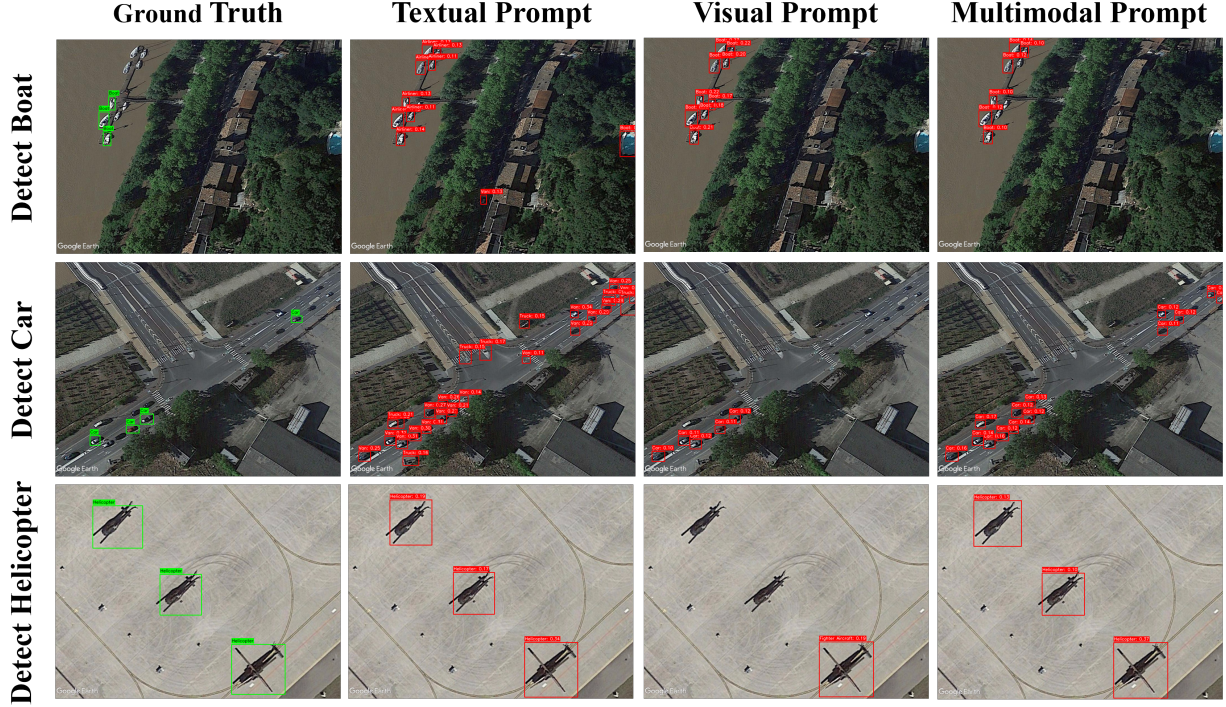


Figure 4. Qualitative comparison of detection results under different prompting strategies. From left to right: ground truth, text-only prompting, visual-only prompting, and multimodal prompting. The three rows illustrate representative scenarios with varying degrees of semantic alignment between pretraining and evaluation: (top) ship detection with category name mismatch (boat vs. ship), (middle) car detection with weak textual representation and confusion with visually similar categories (e.g., van), and (bottom) helicopter detection with strong semantic alignment in pretraining. Multimodal prompting exhibits more balanced behavior across scenarios by combining complementary textual and visual cues.

category semantics are well aligned with pretraining, leading to strong performance under text-only prompting, while visual prompting alone fails to detect some instances due to limited exemplar coverage. Across all scenarios, multimodal prompting achieves more balanced performance by integrating complementary textual and visual cues, demonstrating improved adaptability across diverse semantic conditions.